Nanoarchitecture of Semiconductor Titania Nanosheets Revealed by Polarization-Dependent Total Reflection Fluorescence X-ray Absorption Fine Structure

Katsutoshi Fukuda,[†,‡] Izumi Nakai,[*,†] Chizuru Oishi,[†] Masaharu Nomura,[§] Masaru Harada,[‡] Yasuo Ebina,[‡] and Takayoshi Sasaki[*,‡]

Department of Applied Chemistry, Tokyo University of Science, 1-3 Kagurazaka, Shinjuku, Tokyo 162-8601, Japan, Advanced Materials Laboratory, National Institute for Materials Science, 1-1 Namiki, Tsukuba, Ibaraki 305-0044, Japan, and Photon Factory, Institute of Materials Structure Science, High Energy Accelerator Research Organization, 1-1 Oho, Tsukuba, Ibaraki 305-0801, Japan

Received: May 24, 2004; In Final Form: June 21, 2004

The nanoarchitecture of unilamellar titania nanosheets was studied by X-ray absorption fine structure (XAFS) analysis utilizing two different geometrical arrangements, s- and p-polarization. In total reflection fluorescence mode using synchrotron radiation X-ray, an XAFS signal was detected in high yield for monolayer films of nanosheets having a thickness of only ~10 Å, which were deposited via electrostatic self-assembly. Obtained extended X-ray absorption fine structure oscillations were dependent on the polarization due to the two-dimensional anisotropy of the nanosheets. This dependence was helpful in analysis of the nanosheet architecture, which was conducted on the basis of free energy force field (FEFF) simulations of the parent layered titanate. Satisfactory curve-fitting of the EXAFS data of the unilamellar nanosheet was achieved. The obtained results revealed the elongation of some interatomic distances, particularly those having a component along the nanosheet normal, when compared with the crystal structure data for the parent layered titanate. This structural modification led to 4% expansion in sheet thickness upon exfoliation, which can be understood by mitigation of electrostatic repulsion between titanium ions in the negatively charged nanosheet and its countercations.

Introduction

Titanium oxide is a versatile material with a range of applications, including solar-cells,[1,2] photocatalysts[3,4] and photoinduced wettability.[5] Semiconductor titania nanosheets obtained by exfoliation of a layered titanate[6,7] have received considerable attention as a new family of titania nanomaterials. The unilamellar nanosheets exhibit novel physicochemical properties[8] and thermal-induced structure transformation[9] associated with sheet thickness on a nanometer scale. Recently reported ultrathin films of nanosheets fabricated by electrostatic self-assembly procedure[10,11] will be useful in various applications.

The structural information on the nanosheet crystallites, particularly in an individual state of molecular entities, is of essential importance in understanding and, thus, controlling their chemical and physical properties, because the structure and properties may be modified to some extent once they are restacked to form a "bulk" crystal. Transmission electron microscopy and X-ray diffraction techniques have been applied for structure analysis on exfoliated functional materials such as titania nanosheets,[12] manganese oxide nanosheets,[13] and niobate nanosheets.[14] A two-dimensional characteristic of the unilamellar nanosheets has been demonstrated; they can be described as two-dimensional crystals having periodic arrangements of constituent atoms parallel to the sheets. For example, electron diffraction revealed that the titania nanosheet has a two-dimensional rectangular unit cell (3.0 Å × 3.8 Å). In contrast, diffuse scattering rods were observed along the sheet normal, indicating the absence of periodicity. Although the general structural features have been uncovered by these studies, quantitative information, for example, interatomic distance, is not yet available. Due to the aforementioned importance of the structural information on individual and unilamellar nanosheets, not in a restacked form, a monolayer film of the nanosheets needs to be examined for quantitative structure analysis. A special technique is required to obtain the information from such monolayer samples, because only a very faint signal is expected.

X-ray absorption fine structure (XAFS) composed of X-ray absorption near edge structure (XANES) and extended X-ray absorption fine structure (EXAFS) has been regarded as a powerful clue to obtaining local structural information of noncrystalline materials. These X-ray absorption spectra depend on the direction of the X-ray electric field vector. The amplitude of polarized EXAFS oscillation is correlated with an effective coordination number, N^*, which is expressed by following equation,

$$N^* = 3\sum_i \cos^2 \theta_i \qquad (1)$$

where θ_i is an angle between the polarization vector and the ith bond vector. Recently, polarization-dependent XAFS under X-ray total external reflection mode has been used to characterize the Pt clusters on the single crystal of Al_2O_3[15] and the Mo oxides supported on TiO_2(110).[16] This advanced technique can selectively extract the structural information parallel to the polarization vector of incident X-ray from extremely diluted targets on a substrate when they exhibit a preferred orientation.

* Corresponding authors. (Nakai) Fax: +81-3-3235-2214. E-mail: inakai@rs.kagu.tus.ac.jp. (Sasaki) Fax: +81-29-854-9061. E-mail: sasaki.takayoshi@nims.go.jp.

† Tokyo University of Science.

‡ National Institute for Materials Science.

§ High Energy Accelerator Research Organization.

10.1021/jp047766w CCC: $27.50
Published on Web 08/10/2004

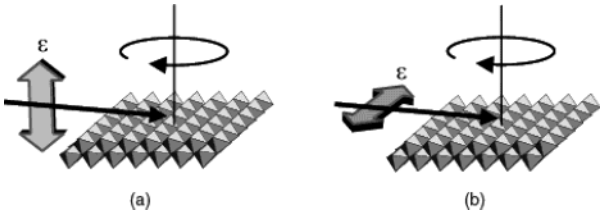

Figure 1. Schematic illustration for (a) p- and (b) s-polarization arrangement of nanosheet film with respect to the incident X-ray with the electric-field vector of ϵ. Note that the nanosheets deposited on the substrate have random orientation within the substrate plane.

These capabilities are expected to be beneficial in ultrathin nanosheet systems (thickness is generally below 10 Å) with a very high two-dimensional anisotropy.

Here, we report the analysis of atomic architecture of titania nanosheets by polarization-dependent total reflection fluorescence X-ray absorption fine structure (hereafter abbreviated as PTRF-XAFS) measurements. Structural changes induced by the delamination are discussed.

Experimental Section

Material Synthesis. A starting layered titanate with a chemical formula of $Cs_{0.7}Ti_{1.825}\square_{0.175}O_4$ ($\square$: vacancy) was synthesized by calcination of a stoichiometric mixture of Cs_2CO_3 and TiO_2 at 800 °C.[17] The product was treated with 1 mol dm^{-3} HCl solution for 3 days to be converted into an acid-exchanged form, $H_{0.7}Ti_{1.825}\square_{0.175}O_4 \cdot H_2O$.[18] A translucent colloidal solution, in which unilamellar titania nanosheets of composition $Ti_{0.91}O_2^{0.36-}$ were dispersed, was obtained by vigorously shaking the acid-exchanged titanate (0.4 g) with a tetrabutylammonium hydroxide ($(C_4H_9)_4NOH$) solution (100 cm^3, 0.016 mol dm^{-3}) at ambient temperature.[6] The nanosheet had an average lateral dimension of 700 nm, and its crystallographic thickness was 7 Å.[12] These titania nanosheets were adsorbed into a monolayer film by electrostatic self-assembly onto a substrate.[10] A quartz glass plate was used as an appropriate substrate for XAFS measurements. It was cleaned by immersing in HCl/CH_3OH (1:1) solution and then in concentrated H_2SO_4 solution, after which it was treated with an aqueous solution of polyethylenimine (PEI, pH = 9, 2.5 g dm^{-3}) for 20 min to precoat the surface with this polycation. Next, the substrate was immersed in the colloidal suspension of negatively charged titania nanosheets (pH = 9, 0.08 g dm^{-3}) for 20 min. Such an operation led to a monolayer film in which the nanosheets lay flat to the substrate.

Measurement and Analysis. PTRF-XAFS measurements were performed at the Photon Factory BL-12C in the Institute of Materials Structure Science, High Energy Accelerator Research Organization (KEK-PF). Synchrotron radiation X-ray was monochromated by Si(111) double crystals. Square beams of 0.2 mm × 2 mm and 0.8 mm × 1 mm were prepared by $X-Y$ slits for s- and p-polarization, respectively, and incident X-ray intensity (I_0) was monitored by an ionization chamber. The incident angle to the sample surface was fixed below the critical angle (~0.35°) for the total external reflection. The fluorescence X-ray intensity (I_f) was detected by a 19-element Ge solid-state detector arranged in the horizontal plane of the substrate. Polarization-dependent measurements were conducted by changing the geometrical configuration of the film with respect to the incident X-ray beam (Figure 1). Ti K-edge XAFS spectra were recorded in an energy range from 4660 to 5850 eV with an interval of 0.3 and 2.2 eV for XANES and EXAFS regions, respectively, at room temperature.

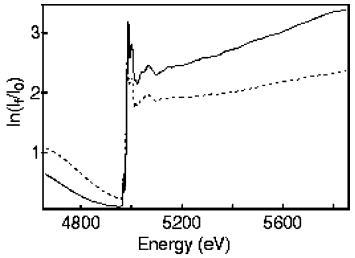

Figure 2. Ti K-edge XAFS spectra of the titania nanosheet taken at p-polarization (broken line) and s-polarization (solid line).

PTRF-XAFS spectra were calculated directly from the intensity ratio of I_f to I_0 without any correction for self-absorption because the sample thickness was negligible. The EXAFS oscillations $\chi(k)$ (where k is the photoelectron momentum) were extracted from the spectra by using a spline-smoothing method performed with the EXAFS analysis program RIGAKU REX2000 (version 2.3.2). The k^3-weighted EXAFS oscillations were then Fourier transformed. The backscattering amplitude and phase function for each shell distance were calculated from reference EXAFS spectra of TiO_2 (rutile), which has similar atomic interactions in terms of species and distance.[19,20] They were used in the curve-fitting analysis for the nanosheet samples. The Debye−Waller factor was first set to 0.0036 $Å^2$ and then optimized considering the coordination number. The goodness of fit was evaluated by a reliability factor calculated as

$$R_f = \sum\{k^3\chi_{obs}(k) - k^3\chi_{cal}(k)\}^2 / \sum\{k^3\chi_{obs}(k)\}^2 \qquad (2)$$

The error of each parameter was estimated from the square root of the diagonal element of the covariance matrix.[21]

Structure analysis for the titania nanosheet was performed by comparing the observed data with the calculated data of $Cs_{0.7}Ti_{1.825}\square_{0.175}O_4$ by free energy force field (FEFF) 8.00, a multiple scattering code for predicting polarized XAFS spectra developed by Rehr et al.[22] The FEFF calculations for the parent titanate were carried out using structural parameters previously reported[17] under the following conditions: S_0^2 (amplitude reduction factor) = 0.8; R_{max} (maximum calculation path length) = 3.5 Å; NLEG (the number of legs, up to six scattering paths with total distances <3.5 Å were evaluated) = 6; δ^2 (Debye−Waller factor) = 0.0036 $Å^2$. The s- and p-polarization effects were also considered in the simulations.

Results and Discussion

When the total reflection mode was utilized, high fluorescence yields could be attained in both polarization arrangements, even from a monolayer of titania nanosheets having a very small thickness of <10 Å (see Figure 2). Note that the sample quantity is very limited: 2.2×10^{-7} g cm^{-2} by assuming a perfect monolayer of the nanosheets with a two-dimensional unit cell (3.8×3.0 $Å^2$) that contains two formula weights of $Ti_{0.91}O_2$. Figure 3 shows polarization-dependent Ti K-edge XANES spectra for titania nanosheets after background correction. The XANES spectra of titania nanosheets exhibited a pre-edge feature consisting of three or four peaks (4964−4974 eV), which was followed by a white line peak (4983−5003 eV). The pre-edge multiple peaks can be assigned to forbidden transitions from the core 1s level to unoccupied 3d states of a tetravalent titanium ion in the distorted TiO_6 octahedron. Similar pre-edge structures have been observed for anatase and rutile,[23−25] although their intensity distribution differed significantly from those of the titania nanosheet with respect to the central upsurge

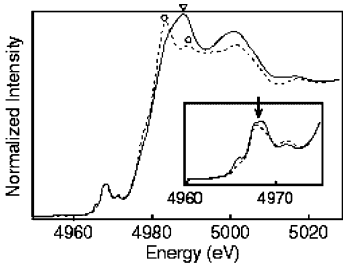

Figure 3. Ti K-edge XANES spectra of the titania nanosheet from p-polarization data (broken line) and s-polarization data (solid line), respectively. Inset shows enlargement of the pre-edge region.

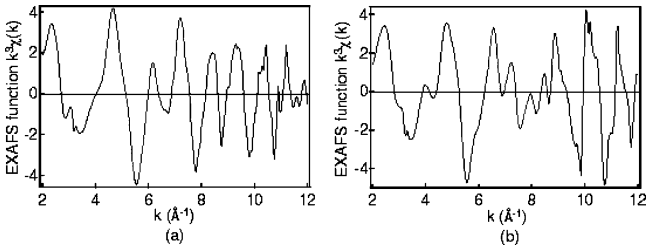

Figure 4. k^3-weighted Ti K-edge PTRF-EXAFS oscillations: (a) p-polarization, (b) s-polarization.

at 4968−4969 eV (shown by arrow in the inset of Figure 3). This may be related to the degree of distortion of the TiO_6 octahedra. Note that the octahedra in the parent layered titanate are appreciably distorted in comparison with those in polymorphs such as anatase and rutile.

Characteristic XANES features were observed in the white line region arising from dipole-allowed transitions from the core 1s to unoccupied 4p states. These features were evidently dependent on the polarization. The p-polarization spectra showed two peaks located at 4983.5 ± 0.3 and 4988.8 ± 0.3 eV (shown by circles in Figure 3), whereas the s-polarization data gave one feature, which appeared at 4987.9 ± 0.3 eV (shown by a triangle). A similar polarization-dependent feature was reported in XANES spectra of a single crystal of rutile.[26] Only one peak at 4987.1 ± 0.1 eV was observed in the spectra where the polarization vector of the X-ray beam was aligned parallel to the extending ribbon of edge-shared TiO_6 octahedra ([001] direction in rutile). In contrast, two transitions at 4983.1 ± 0.1 and 4988.8 ± 0.1 eV were detected in the spectra where the polarization vector was parallel to the [110] direction. This was explained by the distorted symmetry (D_{2h}), which is reflected to the splitting of 4p orbital.[26] There are some similarities in the orientational relationship of the distorted octahedra with respect to polarization vectors between the nanosheet and rutile, which may account for the similar polarization dependence.

EXAFS oscillations $\chi(k)$ also displayed marked dependence on the polarization (Figure 4). This effect is seen more clearly in Fourier transforms (FT) of the k^3-weighted EXAFS oscillations (Figure 5). Two-dimensional anisotropy should be responsible for this feature. For example, one of the most pronounced differences is that a peak at 2.9 Å in p-polarization data is more intense than that at around 3.0 Å in s-polarization data. This suggests that an atomic interaction vector yielding this peak has a smaller angle to the p-polarization vector than to the s-arrangement.

To obtain insight into the peak assignments, the FEFF theoretical profile was calculated for the parent titanate on the basis of the atomic architecture of the host layer[17] listed in Table 1. The strong polarization dependence was similarly found in the FEFF simulations, as displayed in Figure 6, confirming that

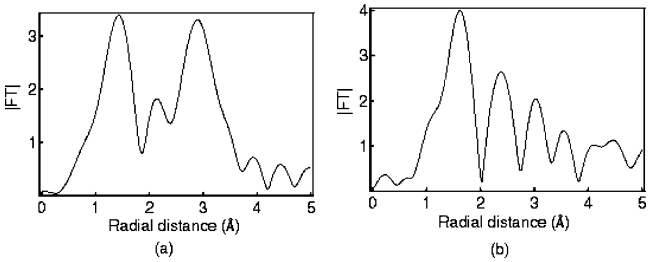

Figure 5. Fourier transforms of $k^3\chi(k)$ spectra in weighting window 3−11 Å^{-1}: (a) p-polarization data, (b) s-polarization data.

TABLE 1: Structural Parameters of Parent Material, $Cs_{0.7}Ti_{1.825}\square_{0.175}O_4$[a]

interaction	N	R (Å)
$(Ti-O)_1$	2.0	1.87
$(Ti-O)_2$	2.0	1.98
$(Ti-O)_3$	2.0	2.13
$(Ti-Ti)_1$	1.8	2.96
$(Ti-Ti)_2$	3.6	3.15

[a] Coordination number N and radial distance R from Ti core.

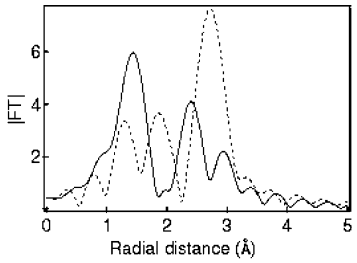

Figure 6. FEFF8.00-calculated FT of $k^3\chi(k)$ spectra for starting layered material in p-polarization (broken line) and s-polarization (solid line).

the two-dimensional structure of lepidocrocite-type is the origin for the dependence. The two Ti−Ti interactions (2.96, 3.83 Å) parallel to the two-dimensional plane do not contribute to the EXAFS oscillation in the case of p-polarization, as is expected by eq 1. The peaks in the p-polarization data of the host layer should be assignable to Ti−O or Ti−Ti interactions having a component along the layer normal, parallel to the *b* axis (Figure 7). The contribution of the $(Ti-O)_2$ interaction is expected to be negligible because a positional displacement along the *b* axis is very small for this atomic pair. Taking these factors into account, FT peaks at 1.3 and 1.9 Å may arise from two Ti−O interactions in the TiO_6 octahedron, $(Ti-O)_1$ and $(Ti-O)_3$, in Figure 7. The Ti atom is displaced from the central position of the octahedron along the *b* axis, leading to two different Ti−O interaction distances. This has been revealed by single-crystal X-ray analysis and can be explained by the strong repulsion between nearest-neighbor Ti^{4+} ions. The strongest FT peak at 2.7 Å can be assigned to this Ti−Ti pair, $(Ti-Ti)_2$, in Figure 7. Note that FT peaks do not necessarily reflect the real interatomic distances, which can be deduced after correction by the phase shift.

On the basis of these assignments of the parent material for $(Ti-O)_1$, $(Ti-O)_3$ and $(Ti-Ti)_2$, a starting model for the EXAFS pattern fitting of p-polarization data of the nanosheets was determined. On the other hand, the FT profile of the s-polarization data provided a complicated interference fringe, since almost all atomic interactions contributed to the EXAFS oscillation. The s-polarization EXAFS data was analyzed by adding the new parameters of the two interactions, $(Ti-O)_2$ and $(Ti-Ti)_1$, to the parameters of the three interactions obtained from the fitting result of the p-polarization data. The best-fitted

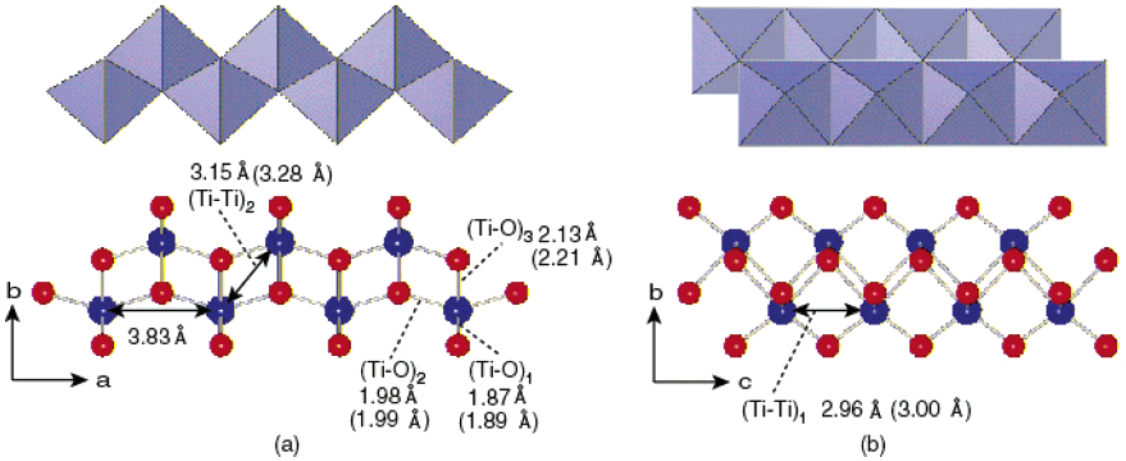

Figure 7. Atomic architecture for the titanate sheet. Projection onto the [001] plane for (a) and [100] for (b). Blue and red circles represent Ti and O atoms, respectively. The axis notation is referred to the orthorhombic unit cell for the original layered titanate. Values without parentheses denote interatomic distances for the precursor layered titanate obtained by single-crystal structure analysis,[17] whereas those in the parentheses indicate the bond length for the nanosheet deduced by the XAFS analysis in this study.

TABLE 2: Structural Parameters of the Titania Nanosheet and Optimized Single Host Layer Based on the First-Principle Study under s- and p-Polarizations

interaction	Ti K-edge EXAFS study					first-principle study[a]	
	N^{*b}		R (Å)				
	p	s	p	s	σ^2 (Å^2)	N	R (Å)
(Ti−O)$_1$	3.1 ± 0.4	1.6 ± 0.6	1.89 ± 0.02	[1.89]	0.004 ± 0.002	2.0	1.82
(Ti−O)$_2$		2.4 ± 1.4		1.99 ± 0.02	0.004 ± 0.003	2.0	1.96
(Ti−O)$_3$	3.0 ± 0.7	1.6 ± 0.9	2.21 ± 0.02	[2.21]	0.004 ± 0.002	2.0	2.22
(Ti−Ti)$_1$		3.6 ± 0.8		3.00 ± 0.03	0.003 ± 0.002	2.0	3.03
(Ti−Ti)$_2$	5.2 ± 1.2	3.0 ± 0.6	3.28 ± 0.01	[3.28]	0.003 ± 0.002	4.0	3.28

[a] See ref 27. [b] Effective coordination number.

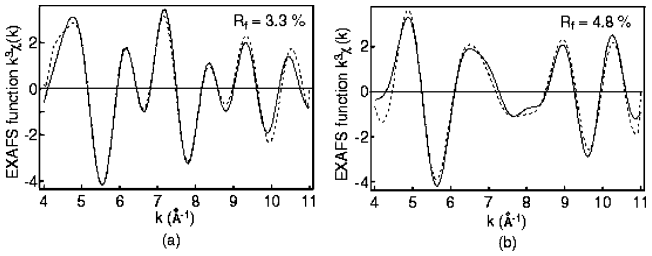

Figure 8. Inverse Fourier transforms of the radial distance from 0.95 to 3.35 Å in (a) p- and (b) s-polarization FT patterns. Solid line and broken line show experimental data and fitting pattern, respectively. R_f is defined by eq 2.

parameters are summarized in Table 2. Inverse Fourier transforms of the radial distance from 0.95 to 3.35 Å in both FT patterns are shown in Figure 8 to demonstrate the high reliability of the fitting.

The titania nanosheet structure was reconstructed on the basis of the local structural parameters obtained by the analysis above. The two-dimensional architecture was confirmed to be preserved after the delamination; a titanium atom has three kinds of coordinated oxygen atoms (each two oxygen atoms) with respect to the bond distance to form a distorted octahedron. The octahedra are combined with each other via edge sharing.

Direct comparison of the nanosheet structure with the starting bulk layered structure indicates that particular interatomic distances, (Ti−O)$_3$ and (Ti−Ti)$_2$, became significantly longer than those in the original bulk structure, while other interatomic distances remained nearly unchanged. The two bonds above align parallel or close to parallel to the sheet normal. Consequently, it was found that exfoliation into the individual sheets brought about 4% expansion of the thickness. This may be accounted for by different locations of charge-compensating species between the nanosheet and its precursor layered crystal. The surface of the negatively charged nanosheets in the monolayer film should be covered with counterions. The most likely cationic species may be tetrabutylammonium ions, which were used as delaminating agent, because the nanosheets were adsorbed onto the substrate from the colloidal suspension containing such a stabilizer. Due to the long alkyl chains (∼7.3 Å when cis−trans conformation is assumed), the positive charge of ammonium ion is located at a long distance (>9 Å) from the titanium ion in the nanosheet. In contrast, in the parent titanate before delamination, interlayer alkali metal ions (Cs^+) and titanium ion are situated much more closely: 3.77 Å as determined by single-crystal structure analysis.[17] Atom positions in the structure should be primarily counterpoised by electrostatic interaction. The displacement of counterions upon exfoliation may allow the increase in Ti−Ti interatomic distance to relax the strong repulsion of this pair. Consequently, the sheet thickness increases. A similar tendency can be found in the layered titanate, which undergoes ion-exchange and hydration reactions. The Ti−Ti interatomic distance is dependent on the size and charge of guest ions and hydration state; e.g., the interatomic distances of hydrated layered titanate accommodating Cs− or K ions as guest species were 3.17 and 3.24 Å, respectively.[18] It should be noted that the structural change upon delamination is the largest when compared with those for the layered crystalline phase induced by ion-exchange and hydration.

Recently, Sato and co-workers carried out structural optimization of the titania nanosheet based on first-principle calculations. The optimized structural data is listed in Table 2 to draw a comparison with the present results.[27] Both sets of data show

excellent agreement, giving elongated interatomic distances along the sheet normal. The calculation was conducted for the hypothetical TiO_2 nanosheet in which the octahedral site is fully occupied with Ti atoms, being in contrast to the real nanosheet with some vacancies at this position. Thus, the nanosheet assumed in the calculation is electrostatically neutral, and counterions were not taken into consideration. The neutral nanosheet may be considered as an extreme case; Ti atoms can move farthest apart from each other without repulsive force from counterions. This may also explain the shorter $(Ti-O)_1$ for the neutral nanosheet.

It is of great interest to clarify how the surface structure differs from the inner part of a material, because such information is essential to understand many important reactions that are driven at a solid surface, for example, heterogeneous catalytic reactions. In this sense, XAFS analysis on nanoparticles has been extensively applied to obtain information on the structural relaxation at a solid surface,[28] which is believed to strongly influence chemical properties, including catalytic activities. Although the contribution from the surface is relatively large for nanoparticles in comparison with bulk substances, it is still sometimes difficult to extract detailed local structural data at a surface. Furthermore, deterioration of crystallinity often observed for ultrasmall particulates prevents precise analysis. In contrast, nanosheet crystallites can be considered as a material composed of all surface atoms without an inner bulk portion. All the constituent atoms are arranged in an ordered fashion to produce a two-dimensional lattice; therefore, the nanosheets may be suitable for exploring how the surface atoms behave. The structural aspects revealed by the present PTRF-XAFS study may provide some insight into understanding the surface structure of solid-state materials.

Conclusion

We analyzed the structure of exfoliated unilamellar crystallite of titanium oxide by applying total reflection XAFS, which could yield high fluorescence. Polarized X-ray from synchrotron radiation source proved to be very helpful for EXAFS analysis of two-dimensional materials such as nanosheets. This study has provided fundamental structural information on titania nanosheets, which will be useful for developing their applications.

Acknowledgment. This work has been supported by CREST of Japan Science and Technology Agency (JST). The total reflection fluorescence XAFS experiments were performed under the approval of the Photon Factory Program Advisory Committee (2001G324). Figure 7 was drawn with VENUS, developed by R. A. Dilanian and F. Izumi (National Institute for Materials Science).

References and Notes

(1) Bach, U.; Lupo, D.; Comte, P.; Moser, J. E.; Weissörtel, F.; Salbeck, J.; Spreitzer, H.; Grätzel, M. *Nature* **1998**, *395*, 583.
(2) He, J.-A.; Mosurkal, R.; Samuelson, L. A.; Li, L.; Kumar, J. *Langmuir* **2003**, *19*, 2169.
(3) Fujishima, A.; Honda, K. *Nature* **1972**, *238*, 37.
(4) Mills, A.; Le Hunte, S. *J. Photochem. Photobiol. A* **1997**, *108*, 1.
(5) Wang, R.; Hashimoto, K.; Fujishima, A.; Chikuni, M.; Kojima, E.; Kitamura, A.; Shimohigoshi, M.; Watanabe, T. *Nature* **1997**, *388*, 431.
(6) Sasaki, T.; Watanabe, M.; Hashizume, H.; Yamada, H.; Nakazawa, H. *J. Am. Chem. Soc.* **1996**, *118*, 8329.
(7) Sasaki, T.; Watanabe, M. *J. Am. Chem. Soc.* **1998**, *120*, 4682.
(8) Sasaki, T.; Watanabe, M. *J. Phys. Chem. B* **1997**, *101*, 10159.
(9) Fukuda, K.; Sasaki, T.; Watanabe, M.; Nakai, I.; Inaba, K.; Omote, K. *Cryst. Growth Des.* **2003**, *3*, 281.
(10) Sasaki, T.; Ebina, Y.; Watanabe, M.; Decher, G. *Chem. Commun.* **2000**, 2163.
(11) Sasaki, T.; Ebina, Y.; Fukuda, K.; Tanaka, T.; Harada, M.; Watanabe M. *Chem. Mater.* **2002**, *14*, 3524.
(12) Sasaki, T.; Ebina, Y.; Kitami, Y.; Watanabe, M.; Oikawa, T. *J. Phys. Chem. B* **2001**, *105*, 6116.
(13) Omomo, Y.; Sasaki, T.; Wang, L. Z.; Watanabe, M. *J. Am. Chem. Soc.* **1998**, *125*, 3568.
(14) Ebina, Y.; Sasaki, T.; Watanabe, M. *Solid State Ionics* **2002**, *151*, 177.
(15) Asakura, K.; Chun, W.-J.; Shirai, M.; Tomishige, K.; Iwasawa, Y. *J. Phys. Chem. B* **1997**, *101*, 5549.
(16) Chun, W.-J.; Asakura, K.; Iwasawa, Y. *J. Phys. Chem. B* **1998**, *102*, 9006.
(17) Grey, I. E.; Li, C.; Madsen, I. C.; Watts, J. A. *J. Solid State Chem.* **1987**, *66*, 7.
(18) Sasaki, T.; Watanabe, M.; Michiue, Y.; Komatsu, Y.; Izumi, F.; Takenouchi, S. *Chem. Mater.* **1995**, *7*, 1001.
(19) Burdett, J. K.; Hughbanks, T.; Miller, G. J.; Richardson, J. W.; Smith, J. V. *J. Am. Chem. Soc.* **1987**, *109*, 3639.
(20) McKale, A. G.; Veal, B. W.; Paulikas, A. P.; Chan, S.-K.; Knapp, G. S. *J. Am. Chem. Soc.* **1988**, *110*, 3763.
(21) Error Reporting Recommendations: A Report of the Standards and Criteria Committee adopted by the IXS Standards and Criteria Committee, 2000.
(22) Rehr, J. J.; Mustre de Leon, J.; Zabinsky, S. I.; Albers, R. C. *J. Am. Chem. Soc.* **1991**, *113*, 5135.
(23) Brydson, R.; Sauer, H.; Engel, W.; Thomas, J. M.; Zeitler, E.; Kosugi, N.; Kuroda, H. *J. Phys.: Condens. Matter* **1989**, *1*, 797.
(24) Ruiz-López, M. F.; Muñoz-Páez, A. *J. Phys.: Condens. Matter* **1991**, *3*, 8981.
(25) Wu, Z. Y.; Ouvrard, G.; Gressier, P.; Natoli, C. R. *Phys. Rev. B* **1997**, *55*, 10382.
(26) Poumellec, B.; Cortes, R.; Tourillon, G.; Berthon, J. *Phys. Stat. Sol.* **1991**, *164*, 319.
(27) Sato, H.; Ono, K.; Sasaki, T.; Yamagishi, A. *J. Phys. Chem. B* **2003**, *107*, 9824.
(28) Chen, L. X.; Rajh, T.; Wang, Z.; Thurnauer, M. C. *J. Phys. Chem. B* **1997**, *101*, 10688.